Measuring Fast Dynamics in Solutions and Cells with a Laser Scanning Microscope

Michelle A. Digman,* Claire M. Brown,† Parijat Sengupta,* Paul W. Wiseman,‡ Alan R. Horwitz,† and Enrico Gratton*

*Laboratory for Fluorescence Dynamics, University of Illinois at Urbana-Champaign, Urbana, Illinois; †Department of Cell Biology, School of Medicine, University of Virginia, Charlottesville, Virginia; and ‡Departments of Chemistry and Physics, McGill University, Montreal, Quebec, Canada

ABSTRACT Single-point fluorescence correlation spectroscopy (FCS) allows measurements of fast diffusion and dynamic processes in the microsecond-to-millisecond time range. For measurements on living cells, image correlation spectroscopy (ICS) and temporal ICS extend the FCS approach to diffusion times as long as seconds to minutes and simultaneously provide spatially resolved dynamic information. However, ICS is limited to very slow dynamics due to the frame acquisition rate. Here we develop novel extensions to ICS that probe spatial correlations in previously inaccessible temporal windows. We show that using standard laser confocal imaging techniques (raster-scan mode) not only can we reach the temporal scales of single-point FCS, but also have the advantages of ICS in providing spatial information. This novel method, called raster image correlation spectroscopy (RICS), rapidly measures during the scan many focal points within the cell providing the same concentration and dynamic information of FCS as well as information on the spatial correlation between points along the scanning path. Longer time dynamics are recovered from the information in successive lines and frames. We exploit the hidden time structure of the scan method in which adjacent pixels are a few microseconds apart thereby accurately measuring dynamic processes such as molecular diffusion in the microseconds-to-seconds timescale. In conjunction with simulated data, we show that a wide range of diffusion coefficients and concentrations can be measured by RICS. We used RICS to determine for the first time spatially resolved diffusions of paxillin-EGFP stably expressed in CHOK1 cells. This new type of data analysis has a broad application in biology and it provides a powerful tool for measuring fast as well as slower dynamic processes in cellular systems using any standard laser confocal microscope.

INTRODUCTION

Recent advances in fluorescent probes including genetically encoded fluorescent fusion proteins and imaging technologies have opened the door to studying dynamic cellular processes in living cells. Ideally, for each molecular entity in the cell, one would like to know its concentration, aggregation state, interactions, and dynamics in different locations within the cell at different times. It has become apparent that many cellular processes are spatially and temporally regulated within the cell (1). New image analysis tools can provide dynamic information as a function of time and space-generating dynamic cellular maps throughout the cell (2). However, in developing these maps we need to move beyond simple averages for large regions of the cell and distinguish the underlying protein distributions that give rise to these averages, i.e., distinguish between a few aggregates containing a large number of molecules and many aggregates that contain a small number of molecules in a well-defined stoichiometry. More important is to have the ability to measure the dynamics of molecular aggregates with lifetimes that could range from small fractions of a second to many seconds.

Optical microscopy methods of increasing sensitivity, resolution and faster frame rate are being developed to generate this type of data. These methods include, among others, fluorescence resonance energy transfer, spectral decomposition, speckle fluorescence microscopy, and lifetime imaging, which can now be applied to living cells. Single-molecule methods have also reached an ultimate sensitivity and time resolution (3–5). However, while single-molecule techniques have had much success on immobilized and isolated systems, their application to molecules in living cells is still challenging. Instead, methods that provide average values, possibly on relatively few molecules in a small volume of the cell, are being used successfully. New developments in image correlation microscopy, based on laser scanning confocal methods and two-photon excitation, have begun to provide this information (2,6). These techniques have been used to develop detailed spatial maps of protein concentrations, dynamics, and interactions, and also to follow the development and dynamics of relatively large molecular assemblies in living cells (2).

Temporal and spatial resolution is a major consideration in correlation microscopy. Single-point fluorescence correlation spectroscopy (FCS), originally developed by Magde et al. (7) and Elson and Magde (8), for the study of molecules in solution, has been extended to two-photon excitation in cells (9) to provide information about protein concentrations and dynamics at high temporal resolution (microseconds) within a very small region of the cell (~1 fL). However,

Submitted March 13, 2005, and accepted for publication May 10, 2005.

Address reprint requests to M. A. Digman, E-mail: mdigman@uiuc.edu; or E. Gratton, E-mail: enrico@scs.uiuc.edu.

0006-3495/05/08/1317/11 $2.00

doi: 10.1529/biophysj.105.062836

point FCS is limited to rapid processes occurring in a single location within the cell. Image correlation spectroscopy (ICS), developed by Petersen et al. (10), is a mathematical image-processing method that can be applied to any kind of microscope (or nonmicroscope) image or stack of images. The basis of the ICS method is to calculate the spatial autocorrelation function of an image using two-dimensional fast-Fourier transform algorithms. The number and size of aggregates is extracted from the analysis of the spatial power spectrum. ICS in cells provides the degree of aggregation and the average number of fluorescently labeled protein aggregates for an entire image. In a recent variation, ICS, termed image correlation microscopy, was expanded to allow temporal correlations between images collected in a time series (11) and to determine spatial correlations due to flow and other cellular processes in regions of the cell (2,6). Temporal ICS operates on image stacks and thus provides spatial maps of molecular interactions and dynamics with a spatial resolution theoretically equal to that of the original image and a time resolution that depends on the frame rate (usually on a timescale of seconds).

In this article we propose a method that has the potential to bridge the gap between the high temporal resolution of single-point FCS (microseconds) and the low temporal resolution of ICS (seconds). The original ICS theory was based on the assumption that the molecules being measured do not move substantially on the timescale of a single image frame acquisition (seconds). So it has been mostly used to study fixed sample or slowly moving transmembrane- or membrane-associated proteins (12). Here we demonstrate that images from laser scanning microscopes (LSM), including a standard commercial single photon confocal and a two-photon excitation microscope, contain a hidden temporal structure. A general mathematical method for analyzing spatial and temporal correlations within images from the rapid scanning of the laser is presented, and shows that LSM images can be exploited to extract fast dynamic information. Specifically methods are developed for the analysis of images generated by either 1), scanning repeated circular orbits or lines, or 2), raster-scanning images of larger areas. Simulations and experiments demonstrate the feasibility of the methods showing that the dynamics of fast molecular diffusion in solution and in the cell can be extracted directly from laser scanning microscopy (LSM) images.

This new analysis, termed raster image correlation spectroscopy (RICS), successfully bridges the timescales of FCS and ICS and provides spatially resolved dynamic information in the microsecond-to-second time range. For raster-scan images the spatial resolution of this method depends on the diffusion coefficient of the molecules or molecular aggregates. The spatial resolution will be lower for rapidly diffusing molecules because they cannot be localized with high precision. To date, expensive and highly specialized instruments have been required for FCS measurements. In addition, the FCS measurements and imaging have to be done at two different times with different conditions. Since LSMs are readily available in almost all life science labs, the RICS method opens up the measurement of fast dynamics within the cell to the general microscope user. On a single instrument from a temporal stack of images one can obtain dynamic information anywhere from the microsecond-to-hours timescale. This includes dynamic processes ranging from that of diffusion of cytosolic proteins to slower processes such as the assembly and disassembly of large multiprotein complexes. The potential impact of RICS on the life science community is enormous, since it allows the determination of spatial maps of concentrations, aggregation, and dynamics in living cells using readily accessible instrumentation.

Temporal and spatial fluctuations in microscope images

We first describe how to measure fast diffusion dynamics of molecules in a dilute, homogenous solution using a conventional LSM. Although images appear uniform, there are hidden temporal and spatial fluctuations that can be analyzed to recover the diffusion coefficient and the number of molecules in the instantaneous (scanning) excitation volume.

Molecular processes such as conformational transitions, and quenching associated with aggregation and molecular rotations, as well as diffusion, can cause fluctuations in fluorescence intensity. However, for this mathematical derivation we only consider signal fluctuations due to diffusion of particles in a homogenous medium since most of the processes in the cell involve transport (either by diffusion or by directed motion) of particles from one location to another. Diffusion of a particle in a uniform medium can be described by the relationship below,

$$C(r,t) = \frac{1}{(4\pi Dt)^{3/2}} \exp\left(-\frac{r^2}{4Dt}\right), \qquad (1)$$

where D is the diffusion coefficient, and $C(r,t)$ is proportional to the probability of finding the particle at position r, at time t, when the particle was at the origin, $r = 0$ at time $t = 0$. The temporal and spatial autocorrelations are derived from Eq. 1. There are two distinct parts of this equation—a temporal part and a spatial exponential Gaussian term. If a particle was at the origin at $t = 0$, it can be found at a distance r from the origin with a Gaussian distribution where the variance depends on time and the diffusion coefficient of the particle. If the concentration is sampled at one position, as is usually done with single-point FCS, the temporal autocorrelation function of the fluorescence intensity decays with a characteristic time that depends on the diffusion coefficient and the size of the illumination volume. Alternatively, the concentration can be sampled at different spatial locations. In this case, the spatial autocorrelation function decays with a characteristic length that depends on the diffusion coefficient and the size of the illumination volume. A detailed

description of how motion of molecules and molecular aggregates influences the spatial correlation function in raster-scanned images was presented recently (13).

LSM using either line-scan or raster-scan modalities enables data acquisition from different spatial locations at different times. Spatial correlations for small diffusing particles depend on the spatial overlap and the time interval between adjacent pixels. Random diffusion of the particle and longer time intervals between data points decrease correlation at shorter spatial scales but increase correlation at distant pixels. It is precisely the change of shape of the spatial correlation function that contains information about molecular diffusion. For the most common scan configurations, circular or line-scan and raster-scan microscopy, the adjacent volumes along the scanning line are sampled very rapidly; but the adjacent volumes in two consecutive lines are sampled at a much slower rate. This difference in sampling time can be exploited to measure a range of diffusion coefficients, from very fast molecular diffusion through the illumination volume, which occurs in the microsecond range to slower diffusion, which can occur on the timescale of milliseconds or even seconds.

Starting from Eq. 1, the relationship between the concentration of a particle and fluorescence intensity F is given by

$$F(t) = \kappa Q \int d\mathbf{r}\, W(\mathbf{r})\, C(\mathbf{r}, t), \tag{2}$$

where the integral is calculated over the entire excitation volume, Q is the quantum yield, κ is a factor that accounts for the instrument sensitivity, and $W(\mathbf{r})$ describes the point-spread function (PSF) of the microscope system. In Eq. 2, the concentration of the particle as a function of time (Eq. 1) is convolved with the expression for the illumination profile $W(\mathbf{r})$. The temporal autocorrelation function (ACF) is given by the expression below,

$$G(\tau) = \frac{\langle \delta F(t) \delta F(t+\tau) \rangle}{\langle F(t) \rangle^2}. \tag{3}$$

In this equation the angled brackets indicate time averages; δF is the fluorescence intensity fluctuation with respect to the average, and τ is the delay time between successive sampling of the fluorescence signal. By inserting Eq. 2 into Eq. 3 and assuming time sampling at the same spatial locations (see, for example, Eq. 7 below), we can obtain the familiar autocorrelation function used in FCS for the analysis of a particle freely diffusing in a volume.

To derive expressions for the spatial autocorrelations we need to specify the spatial sampling sequence used in the experiment. Equations for the spatiotemporal correlation function for data were generated using two common modalities, from which a circular (line) or raster scan pattern will be derived. These equations are then used to fit experimental spatiotemporal correlation functions and diffusion coefficients, and the concentrations of molecules in dilute samples are extracted.

Temporal correlations in circular scanning

If the scanner performs a circular orbit of radius A and angular frequency ω around a center at x_0 and y_0, the relationship among x, y, and the time is given by the sine and cosine functions, respectively, as

$$\begin{aligned} x(t) &= x_0 + A \times \sin(\omega t) \\ y(t) &= y_0 + A \times \cos(\omega t). \end{aligned} \tag{4}$$

These expressions are used to describe the position of the PSF term $W(\mathbf{r})$ in Eq. 2, which is now time-dependent. If molecular diffusion and laser scanning are independent (as they should always be unless the light affects the motion of the particle), then the convolution integral in Eq. 2 splits into the product of two functions when the autocorrelation function is evaluated,

$$G_S(\tau) = S(\tau) \cdot G(\tau). \tag{5}$$

$S(\tau)$ is the autocorrelation function due to scanning and $G(\tau)$ the autocorrelation function without scanning. Assuming a three-dimensional Gaussian excitation profile with a radial waist w_0 and axial waist w_z, the S(τ) term for circular scanning is given by

$$S(\tau) = \exp\left(-\frac{4A^2(1-\cos(\omega\tau))}{\left(1+\frac{4D\tau}{w_0^2}\right) w_0^2} \right). \tag{6}$$

$G(\tau)$ is the familiar autocorrelation function due to diffusion,

$$G(\tau) = \frac{\gamma}{N}\left(1+\frac{4D\tau}{w_0^2}\right)^{-1}\left(1+\frac{4D\tau}{w_z^2}\right)^{-1/2}. \tag{7}$$

Equations 6 and 7 combined with Eq. 5 are used to fit the autocorrelation functions from circular-scan experiments to extract the diffusion coefficient, D, of the particle using the geometrical factors that describe the beam profile (w_0 and w_z), i.e., the radius of the orbit A and the angular frequency ω of circular scanning (14). Note that Eqs. 6 and 7 contain only the time, τ. In this analysis the spatial correlation between adjacent points in the orbit and successive orbits is hidden.

Spatial correlations in circular, line, and raster scanning

To reveal the spatial part of the correlation function and to show the similarity between RICS and ICS we construct a transpose matrix from the time series in which each column represents points along the circular orbit (or line) and each row represents a different orbit (or line). This transpose matrix is a pseudo-image of the orbit because the vertical axis is not space but time. The entire time series is then divided into a pseudo-image stack of frames in a 2^n format

that is amenable for calculating the spatial autocorrelation using fast-Fourier transform methods, e.g., 128 × 128 or 256 × 256. The advantage of this image representation is that the spatial and temporal parts of the pseudo-image are separated. For orbit-scanned images, the time data is continuous along the scan and the division of the time series into images gives no particular advantages when studying solutions. However, for line scan or raster scan, the time series is not usually continuous in successive points due to line retracing; the image, in contrast, is contiguous among adjacent points. Therefore, we can apply the spatial correlation operation to the images (the points are equally separated in space), although we cannot apply the correlation operation to the time series obtained in the raster acquisition mode (the points are not equally separated in time). The spatial correlation function is defined as

$$G_S(\xi,\psi)=\frac{\langle I(x,y)I(x+\xi,y+\psi)\rangle_{x,y}}{\langle I(x,y)\rangle^2_{x,y}}, \tag{8}$$

where ξ and ψ are the spatial increments in the x and y directions, respectively, and the angle bracket indicates average over all the spatial locations in both x and y directions. We then calculate the spatial autocorrelation of the raster-scan pseudo-image. The two-dimensional spatial autocorrelation function for circular or line scan is given by

$$S(\xi,\psi)=\exp\left(-\frac{\frac{1}{2}\left[\left(\frac{2\xi\delta r}{w_0}\right)^2\right]}{\left(1+\frac{4D(\tau_p\xi+\tau_l\psi)}{w_0^2}\right)}\right), \tag{9}$$

$$G(\xi,\psi)=\frac{\gamma}{N}\left(1+\frac{4D(\tau_p\xi+\tau_l\psi)}{w_0^2}\right)^{-1}\times\left(1+\frac{4D(\tau_p\xi+\tau_l\psi)}{w_z^2}\right)^{-1/2}, \tag{10}$$

for the S and G parts, respectively. In Eqs. 8 and 9, x and y are the horizontal and vertical coordinates of the image or pseudo-image, respectively, δr is the distance between adjacent points in the line or along the orbit, and τ_p and τ_l are the pixel sampling time and time between lines, respectively. Analogous to Eq. 5, the overall spatial autocorrelation function is given by $G_S(\xi,\psi) = S(\xi,\psi) \times G(\xi,\psi)$.

Raster-scan image correlation spectroscopy

To make RICS accessible to most researchers using standard confocal microscopes, we expanded the theory developed for circular (or line) scan to two-dimensional spatial raster-scan images. In this case, the spatial part of the correlation function is expressed directly in terms of the pixel size, δr (typically in the range 0.05–0.2 μm); pixel resident time, τ_p (typically in the range 2–100 μs); and the line repetition time, τ_l, typically in the 3–100 ms range:

$$S(\xi,\psi)=\exp\left(-\frac{\frac{1}{2}\left[\left(\frac{2\xi\delta r}{w_0}\right)^2+\left(\frac{2\psi\delta r}{w_0}\right)^2\right]}{\left(1+\frac{4D(\tau_p\xi+\tau_l\psi)}{w_0^2}\right)}\right). \tag{11}$$

The overall correlation function is given by $G_S(\xi,\psi) = S(\xi,\psi) \times G(\xi,\psi)$ where $G(\xi,\psi)$ is given by Eq. 9. (Note: All terms containing the diffusion coefficient, D, in Eqs. 9–11 contain a factor of $4D$, but for two-photon excitation this factor should be $8D$. Also, w_0 in all equations of this manuscript is the $1/e^2$ of the illumination Gaussian profile.)

To test the validity of the expressions used to fit the two-dimensional autocorrelation functions, we performed simulations of particles diffusing in a three-dimensional grid. For particles moving at two different rates (diffusion constants of 100 and 6 $\mu m^2/s$), simulations were performed for three illumination scenarios: 1), a stationary beam (standard FCS); 2), a beam rotating in a circular orbit; or 3), a beam moving in a raster-scan fashion. (The simulation program for FCS data has been previously described, and it can be downloaded from https://lfd.uiuc.edu.) Briefly, a number of particles are simultaneously moved in a random walk, at different rates, on a three-dimensional grid with 0.05 μm per grid step. The grid is illuminated with a selected illumination profile function either for one-photon or two-photon experiments. For all simulated data the input parameters were recovered within the noise using the equations presented above (Fig. 1 and Table 1). (See Table 3, later in this article, for an estimation of the noise under the conditions of the simulation for similar values of the total length of the experiment.)

For raster-scan patterns, the correlation of a series of images appears on three different timescales (Fig. 2 *B*). Pixels are microseconds-apart in the horizontal direction, milliseconds-apart along the vertical axis (line-to-line), and seconds-apart between successive frames. The expressions for the correlation function for pixels in different image planes are not contained in Eqs. 10 and 11. They are simply the familiar temporal autocorrelation function given by Eq. 7 where the sampling time is the frame repetition time.

MATERIALS AND METHODS

Confocal images were collected on an Olympus Fluoview 300 microscope (Olympus, Tokyo, Japan) equipped with an I × 70 inverted microscope fitted with a 60× PlanApo (1.40 NA) oil-immersion objective. Excitation was from the 488-nm laser line of a 40-mW Ar ion laser (Melles-Griot, Carlsbad, CA) attenuated to 0.2% power using ND filters and an acoustic optic-tunable filter. A Q500LP dichroic mirror was used for the laser excitation and for collection of the emission from EGFP-labeled cells. The 512 × 512 images were collected using the Fluoview software at 5× zoom, corresponding to a pixel resolution of 0.09207 μm. Under these conditions the pixel dwell-times were 2 μs/pixel (fast scan), 4 μs/pixel (medium scan), or 8 μs/pixel (slow scan), and the time between lines was 1.608 ms (fast scan), 2.12 ms (medium scan), and 3.15 ms (slow scan).

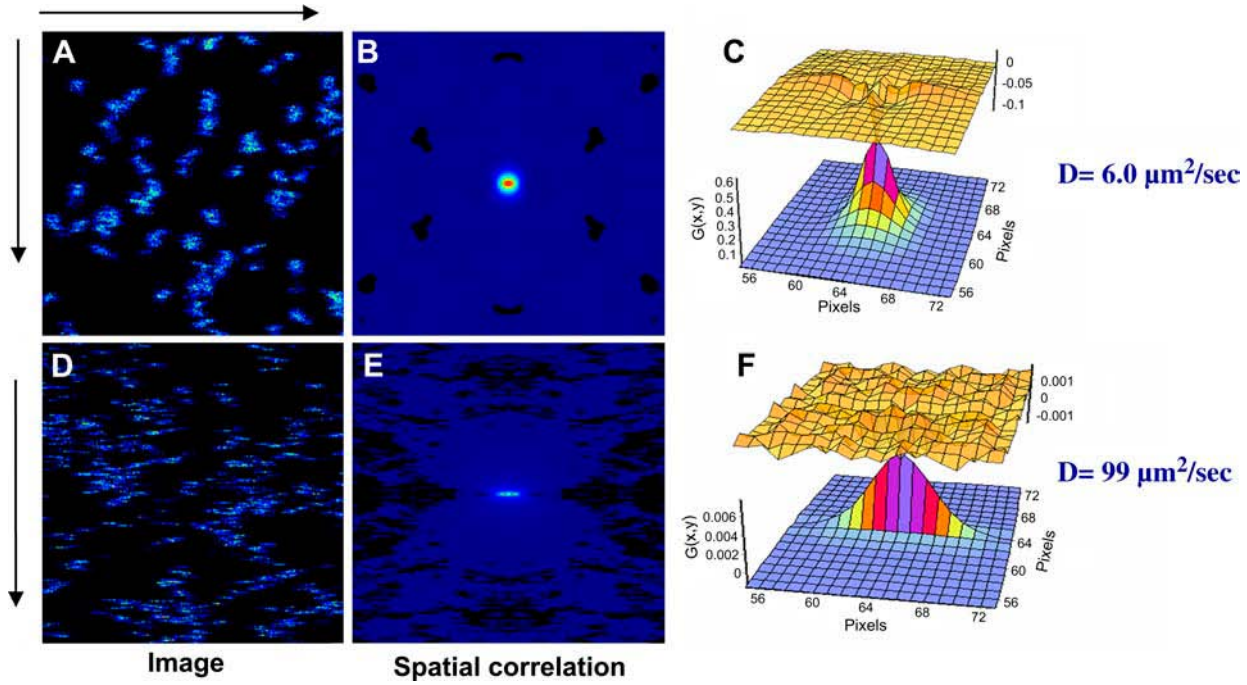

FIGURE 1 Simulated images of freely diffusing 10-nm beads (*A*) and EGFP (*D*) in a plane. The fast EGFP moving molecules appear as a streak in the image (*D*). *B* and *E* are the two-dimensional spatial correlation functions of images *A* and *D*, respectively. *C* and *F* are the fit of the autocorrelation functions *B* and *E* according to the equations in the text. Image parameters: frame 256 × 256, 16 μs pixel time, and 0.050 μm pixel size.

The two-photon excitation scanning fluorescence microscope used in these experiments was assembled at the Laboratory for Fluorescence Dynamics (University of Illinois at Urbana-Champaign) and has been described previously (9). Basically, 100-fs pulses from a mode-locked titanium-sapphire laser (Tsunami; Spectra-Physics, Palo Alto, CA) were used for excitation. The laser was guided into the microscope by *x*,*y* galvano-scanner mirrors (Model 6350; Cambridge Technology, Cambridge, MA), which allowed the beam to move in both the *x* and *y* directions. The mirrors are driven in a preset scanning path using the ISS 3-axis card (ISS, Champaign, IL) and synchronized with data acquisition using the ISS-FCS dual-channel card. Data are acquired and processed by the SimFCS software developed at the University of Illinois. For scanning in a circular orbit, the *x*- and *y*-scan mirrors are driven by two identical sine waves with a 90° phase-shift. The radius and frequency of the circular scan was controlled by the amplitude and frequency of the sine wave. For a raster scan, the *x*- and *y*-scanner mirror was driven by two sawtooth signals at different frequencies. A photomultiplier tube (HC120-08, Hamamatsu Photonics, Bridgewater, NJ) was used for light detection in the photon-counting mode. A BG39 optical filter was placed before the photomultiplier for efficient suppression of IR excitation light. A 40× water immersion objective (Zeiss, Jena, Germany) with 1.2 NA was used for the measurement. The excitation wavelengths used in the study are 780 nm (for polystyrene beads) and 910 nm (for EGFP). Due to the possible variation in the laser alignment from day to day, the waist (w_0) of the excitation beam was calibrated before each day's measurement. The calibration was achieved by measuring the autocorrelation curve of 10 nM fluorescein in 0.01M NaOH, which was in turn fit with a diffusion rate of 300 μm^2/s; the typical values of w_0 were in the range of 0.30–0.50 μm, depending on the laser wavelength. The value of w_z for the one-photon experiment was assumed to be three-times the radial waist and five-times the radial waist for the two-photon measurements.

TABLE 1 Simulations: comparison between three different methods to recover *D* and *G*(0) for two different values of *D* (100 μm^2/s and 6 μm^2/s)

	Single point (Eq. 7)	Circular scan (Eq. 8)	Raster scan (Eq. 10)
D(μm^2/s)	100	100	99
G(0)	2.1	2.0	2.1
D(μm^2/s)	6.6	6.2	6.1
G(0)	2.1	2.0	2.1

Sampling frequency was 128 kHz for the fast moving particle and 32 kHz for the slowly diffusing particle. The orbit was sample at 128 points and the frame for the raster scan was 128 × 128 pixels. 1.6 M points were simulated in each run irrespective of the sample frequency.

For two-photon excitation, scanning fluorescence imaging data were collected at the rate of 16–128 μs/pixel. The scan area for a full frame (256 × 256 pixels) corresponds to 32 × 32 μm. The average fluorescence intensity of the sample remained constant, indicating the fluorophore was not photobleached significantly during the measurement. Some diffusion measurements were made on 10-nm fluorescently-labeled polystyrene beads (Molecular Probes, Eugene, OR) that were diluted in nanopure water and sonicated for 2 h.

CHO-K1 cells stably transfected with paxillin-EGFP were cultured in a humidified, 8.5% CO_2 atmosphere at 37°C in minimum essential medium supplemented with 10% FBS, non-essential amino acids, and glutamine, as well as 0.5 mg/mL neomycin (G418), to maintain selection of transfected cells. Cells were lifted with trypsin and plated on homemade 35-mm glass-bottomed dishes coated with 2–10 μg/mL fibronectin. Cells were maintained in CCM1 medium (HyClone, Logan, UT) at 37°C during imaging with a Warner Instruments heated stage insert (Warner Instruments, Hamden, CT), in combination with a Bioptechs (Bioptechs, Butler, PA) objective heater.

All data fits were performed according to Eqs. 9–11 using the SimFCS program (available at www.lfd.uiuc.edu). When possible, the data was weighted by the standard deviation of the correlation function at each pixel. When a stack of images was available, the spatial autocorrelation function was calculated for each image or image region. The average spatial

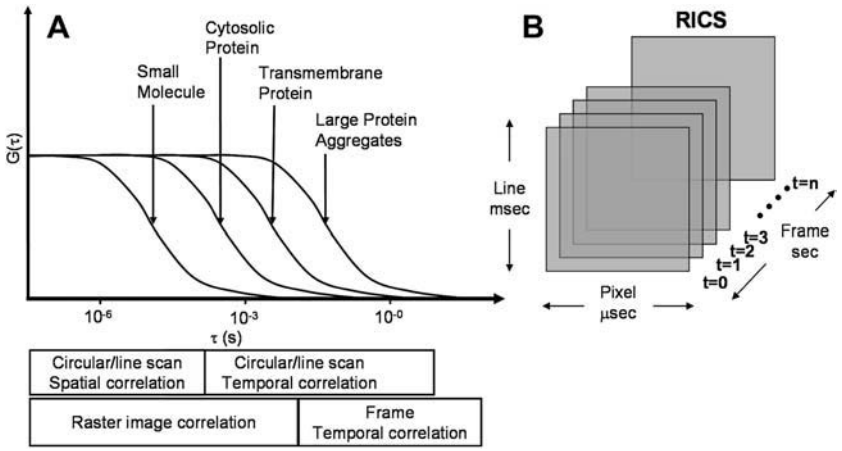

FIGURE 2 Diagram of the range of diffusion times accessible by different scanning techniques. Depending on the timescale of the process, pixel (microseconds), line (milliseconds), or frame (seconds) correlation methods can be used.

correlation function was then calculated and for each point of the spatial correlation function the standard deviation was evaluated and used as the weighting factor. For the time correlation, the time series was broken in segments. The average correlation function was calculated from the autocorrelation function of each segment and the standard deviation of the average at each point was used as the weighting factor for the χ-square evaluation.

RESULTS

Solution experiments

For solution experiments, each sample was measured using three different modalities: 1), point FCS; 2), circular scanning; and 3), raster scanning. Fitting of the autocorrelation function obtained from single-point FCS of freely diffusing 10-nm beads (Fig. 3 *A*) yields a diffusion co-efficient of $\sim$6 $\mu m^2/s$ (Table 2). Similarly, the spatial autocorrelation function (Fig. 3 *C*) of the pseudo-image of the transposed data stream from circular scanning of the same 10-nm bead sample (Fig. 3 *B*) was fit according to according to Eqs. 6 and 7 (Fig. 3 *D*, Table 2). The fitting yields a *D*-value of 8 $\mu m^2/s$ (Table 2). Finally, raster-scan data of the same sample (not shown) yields a similar *D*-value (Table 2).

An image of EGFP in solution collected with a commercial LSM (Fluoview 300, Olympus) shows no visible features (Fig. 4 *A*). However, the two-dimensional spatial correlation function (Fig. 4 *B*) fit with the RICS analysis (Fig. 4 *C*) reveals the hidden structure and the fit to Eqs. 8 and 9 yields the expected diffusion co-efficient for EGFP in solution, $D = 89\ \mu m^2/s$ ($D = 90 \pm 5\ \mu m^2/s$ from single-point FCS). To our knowledge, this is the first time that the fast diffusion of a molecule in solution has been measured using a commercial LSM.

Correlation measurements in cells

Images of cells often contain large immobile structures which will dominate the spatial correlation function and hide other potentially more meaningful information. If fast moving molecules or molecular aggregates move in the presence of these bright immobile features they can be very difficult to see. The immobile features can be filtered out of the images by subtracting, pixel by pixel, the average image calculated using the entire image stack before performing the correlation analysis (similar to Eq. 6). However, after this operation, the average image intensity of each frame of the stack is near zero (the denominator in Eq. 7) and the autocorrelation functions tend to oscillate widely. To circumvent this problem the average image intensity of the entire stack (a scalar) is added to all pixels for each image of the stack. The spatial correlation functions calculated after these operations contain only information about the moving particles. It is important to note that the magnitude of the correlation

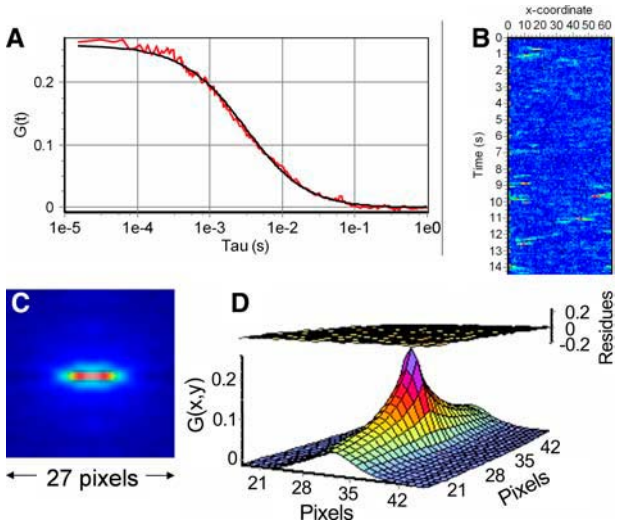

FIGURE 3 10-nm fluorescent beads freely diffusing in solution. (*A*) Single-point FCS. (*B*) Pseudo-image obtained with circular scan. Orbit period is 1 ms, there are 64 points per orbit, and 100 orbits are averaged together per each line of the pseudo-image. The orbit diameter was 1.5 μm. (*C*) Two-dimensional spatial correlation of the pseudo-image. (*D*) Fit of the two-dimensional correlation using the equations in the text.

TABLE 2 Experimentally recovered values of 10-nm beads freely diffusing in solution

	Point FCS (Eq. 7)	Scanning FCS (Eq. 6)	Scanning FCS (Eq. 8)	Raster scan (Eq. 10)
$D(\mu m^2/s)$	5.9	8.4	8.2	8.6

function, $G(0,0)$, is no longer equal to the inverse of the number of molecules; however, relative $G(0,0)$ values from different parts of the cell can still be compared.

Paxillin-EGFP in CHOK1 cells localizes to bright finger-like features that are cellular adhesions (Fig. 5 *A*). A subregion of the cell where most of the paxillin protein is soluble in the cytosol was analyzed (Fig. 5 *B*). There is a contribution in this image from small paxillin-containing adhesions in the central regions of the cell that will dominate the spatial ACF so that the fast dynamics of soluble paxillin cannot be extracted (Fig. 5 *C*). However, after applying the subtraction algorithm, the spatial ACF only reveals the fast moving components (Fig. 5 *D*) and that function can be fit (Fig. 5 *E*) yielding a diffusion coefficient of $D = 8.3\ \mu m^2/s$ (comparable to point-scan FCS measurements, not shown). Different regions of the cell with various shapes, brightness, and total number of dim organized structures were analyzed using the subtraction method and similar D-values were obtained. These regions did not contain bright structures due to large elongated focal adhesions.

In areas of the cell with these large adhesions (Fig. 6, *A* and *B*), the spatial correlation function is dominated by

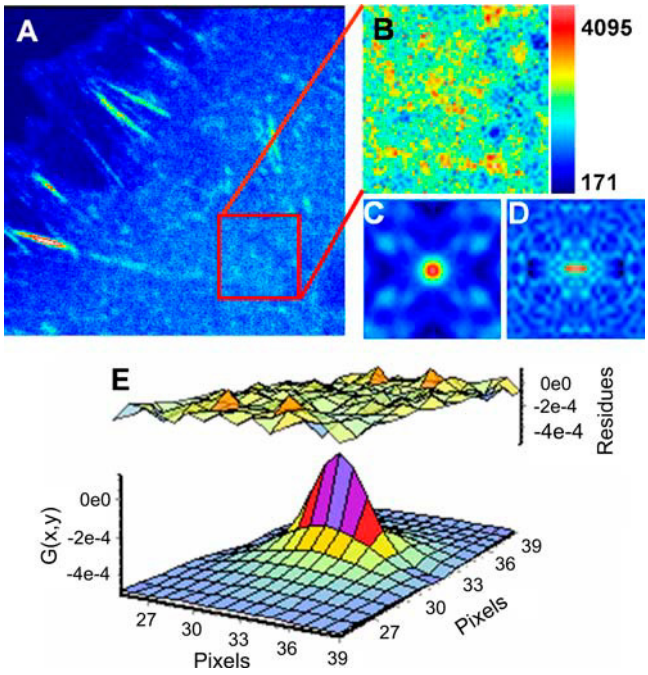

FIGURE 5 (*A*) Image of a CHOK1 cell expressing paxillin-EGFP. (*B*) 64 × 64 subframe in the cytosolic part free of focal adhesion structures. (*C* and *D*) Spatial autocorrelation before (*C*) and after (*D*) subtraction of immobile structures. (*E*) Fit of the spatial correlation function in *D*. The diffusion coefficient in this cell region is 8.3 $\mu m^2/s$. Pixel rate was 8 μs, pixel size is 0.09207 μm, line time is 5.048 ms, frame size 512 × 512, and a total of 23 frames were collected.

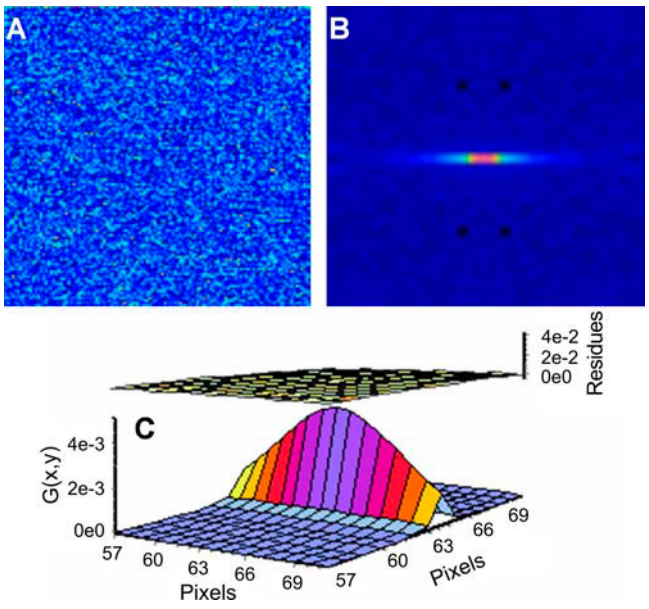

FIGURE 4 EGFP freely diffusing in solution. (*A*) Image obtained with an Olympus LSM. (*B*) Two-dimensional spatial correlation of a stack of images. (*C*) Fit according to the equations in the text. The recovered diffusion coefficient is $D = 89\ \mu m^2/s$. Pixel dwell-time is 4 μs, line time is 3.176 ms, pixel size is 0.09207 μm, and image size is 128 × 128 cut from the original 512 × 512. The protein concentration was 20 nM.

spatial correlations, from these structures masking any correlations due to fast dynamics (Fig. 6 *C*). Remarkably, after the immobile component removal, the mobile ACF is revealed (Fig. 6 *D*) and can be fit (Fig. 6 *E*) to yield an apparent diffusion coefficient of $D = 0.49\ \mu m^2/s$. This diffusion is substantially lower than the diffusion coefficient obtained in cytoplasmic locations, which lacked large adhesions or other large, immobile structures.

Another modality available on standard confocal microscopes and analogous to repeated circular scanning of an orbit is line scanning. This method can be used to further investigate spatial heterogeneity in paxillin dynamics with higher spatial resolution on the millisecond timescale. A line across a region of a CHOK1 cell expressing paxillin-EGFP was repeatedly scanned (Fig. 7, *A* and *B*). The line has 512 points and was repeated at 5.42 ms. A pseudo-image (256 points are shown) of the repeating scan of the line shows brighter areas where the laser images paxillin within adhesions and dimmer regions where paxillin is mostly soluble in the cytosol (Fig. 7 *A*). The RICS analysis values of the diffusion coefficient at different points along the scan line (shown in *green*) reveal large heterogeneities in paxillin dynamics across the cell. There is a clear correlation between fast diffusion in the cytosolic regions where bright structures are absent and slower apparent paxillin dynamics in/near adhesions. Thus, for the first time (to our knowledge) we

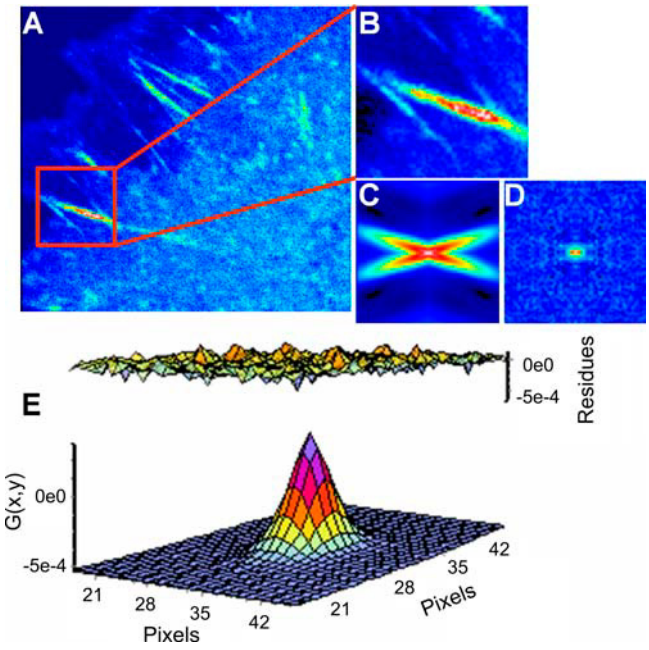

FIGURE 6 (*A*) Image of a CHOK1 cell expressing paxillin-EGFP. (*B*) 64 × 64 subframe in the cytosolic part on a focal adhesion structure. (*C* and *D*) Spatial autocorrelation before (*C*) and after (*D*) subtraction of immobile structures. (*E*) Fit of the spatial correlation function in *D*. The diffusion coefficient in this cell region is 0.49 $\mu m^2/s$. Image parameters are the same as in Fig. 5.

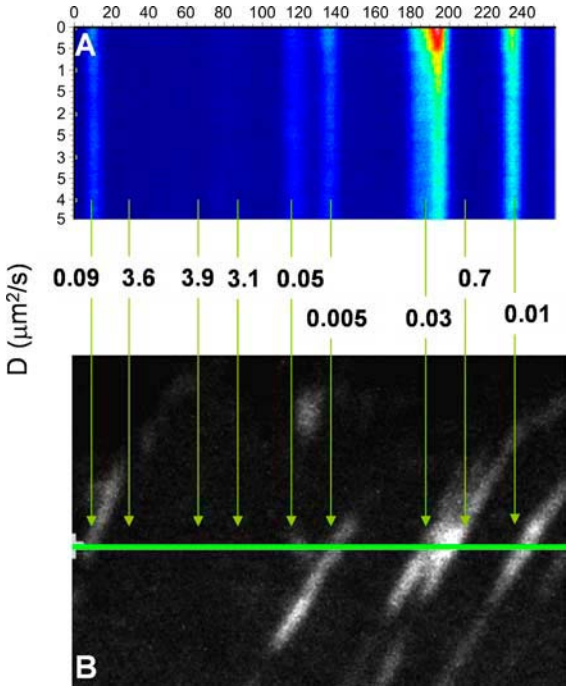

FIGURE 7 (*A*) Pseudo-image of the line scan (*green line* in *B*) of a CHOK1 cell expressing paxillin-EGFP. The image has 512 × 512 pixels. The pixel size is 0.09207 μm. The line time is 5.04 ms. Data were processed according to the equations in the text. For each point along the line the temporal autocorrelation function was calculated and fit using Eq. 7. The recovered values of D (in $\mu m^2/s$) are given at selected positions along the line. There is a clear correlation between low diffusion values and visible structures in the images corresponding to focal adhesion sites.

have been able to generate a high spatial resolution map (limited by the PSF of the microscope) of the fast dynamics of a protein in a living cell. Most notably, this information was obtained by applying the RICS methodology to images collected on a commercial LSM and not a highly specialized instrument.

DISCUSSION

In this article we present an analysis method, RICS, which exploits the hidden time structure of LSM images to recover the values of the rapid diffusion of proteins in both solution and cells. From the mathematical point of view, RICS is basically an extension of the original ICS idea; however, it is not limited to slow dynamics. We also show how circular- and line-scan FCS are related to the RICS technique. Originally circular-scan FCS was introduced to increase the *S*/*N* ratio in measurements of dilute samples (9). When circular- (or line-) scan FCS is applied to cells, it is possible to extract spatiotemporal correlations to obtain very high temporal and spatial resolution maps of intracellular dynamics. For data acquired with the raster technique, we must first represent the data in a contiguous image (or pseudo-image in the case of line scan) and then apply the spatial correlation method. We were able to derive analytical equations for spatial correlations that contain explicitly the effect of molecular diffusion. These equations are then used to fit the experimental spatial correlation functions to extract the diffusion of molecules and molecular aggregates. The range of diffusion coefficients that can be measured is determined by the sampling rates, which are in the microsecond range in common LSM systems, a value adequate to recover the diffusion of a small protein in solution such as EGFP. Therefore, they are more than fast enough to detect the dynamics of proteins within the cell. The form of the equations describing spatial correlations is somewhat similar to the equations used for fitting FCS data in the presence of flow (15). This is not a surprise since either moving the sample or moving the laser beam at a constant velocity should be equivalent. The main difference is that a volume adjacent to the original volume can be explored during the next line of the raster-scan pattern in the RICS method opening up another intermediate timescale.

When the RICS technique is applied to cells, spatial correlations can be dominated by immobile features in the image. A simple algorithm that subtracts the immobile features is sufficient to eliminate the effect of these structures even if they are bright. This is the equivalent of performing a highpass filter operation on the image before applying the spatial correlation algorithm. The highpass filter cutoff can be tuned to subtract slowly moving features. Bright

immobile cellular features are characterized by large shot noise. Dim, fast diffusing particles in the presence of large noise are difficult to see. However, shot noise per se has neither spatial nor temporal correlation so that it can be effectively subtracted without affecting the dynamic information. To account for slowly moving features in the cell, the highpass filter must be tuned to slightly higher frequencies. This filtering operation introduces additional correlations into the data that will be discussed elsewhere. Also in this article we have not examined spatiotemporal correlations to obtain information regarding flow, aggregation, and other dynamic processes such as binding equilibrium occurring in cells. Flow and aggregation processes have been discussed previously in the context of FCS and ICS (2,6).

Comparison of diffusion constants obtained by single-point FCS versus RICS

An important technical question is whether or not the RICS technique is equivalent to standard FCS performed at specific points in solution or in a cell. The time series provided by a laser-scanning microscope, when properly analyzed using the spatial correlation algorithm, basically gives the same information. The RICS technique provides very similar information in regard to the dynamics but is better suited for very low concentrations because it has better *S*/*N*, since many spatial points are sampled in rapid succession. Table 3 shows the results of repeating a simulation of 100 particles diffusing in a plane and detected either by single-point FCS, circular scanning, or raster scanning. Due to the enhanced *S*/*N* the standard deviation of D and $G(0)$ from 10 independent measurements is lower when the RICS technique is applied (Table 3).

Scaling the sampling time, pixel size, and frame size

In the RICS technique measurements must be made at a scan rate that is compatible with the diffusion or other dynamics to be measured. In single-point FCS this requirement is less important because the time series is continuous and if the sampling is fast enough and for a sufficiently long time, all timescales are included. In single-point FCS the instrument parameters are fully specified by the sampling time and the width of the PSF (see Eq. 7). In the scanning method the time series is broken at regular intervals due to retracing. Therefore data must be properly transposed in images according to the line length to apply the spatial correlation algorithm. When compared to single-point FCS, the scanning equations describing spatial correlation depend on two additional instrumental parameters: the pixel size and the line repetition time (see Eqs. 9–11). If the scan rate is too fast, the beam will move out of the region occupied by the molecule before the molecule moved. However, there is another chance to explore an adjacent volume on the next raster line. If the line length is very long (for example 1024 or 2048 pixels) the beam could return to the adjacent volume too late when the probability to find the particle there is small. In general, faster line repetition time and shorter line length are preferred. To illustrate this point, consider a molecule diffusing with a diffusion coefficient $D = 100$ $\mu m^2/s$. The characteristic transit time is ~0.6 ms for a PSF of 0.5 μm full-width at half-maximum. If we sample at 2 μs per pixel and the pixel size is large, the beam could be out of the volume occupied by the molecule before there is appreciable change of the molecule's position. And if the line repetition time is greater than several milliseconds, the particle will not be there when the beam returns on the next line. In general, this effect is important only for fast moving particles and long line lengths. For slower particles there is always a chance to observe the particle again at the next line. If particles are moving very slowly, then the particle motion can be analyzed by correlating successive image frames (11). Table 4 reports the possible correlations and timescales that can be achieved by LSM. In regard to spatial resolution for the determination of dynamics, if the dynamic is slow enough that we can use temporal correlation at one pixel (in the millisecond range or slower); then the spatial resolution is the pixel or the PSF ($\sim<0.5$ μm). Instead, if the dynamics (diffusion) is very fast (in the microsecond to millisecond range), we can use the spatial-correlation approach. This approach uses an area (for example, 16×16 pixels or 32×32 pixels, typically 0.092 μm/pixel) to recover the diffusion parameters, thereby reducing the spatial resolution to the size of that area (limit of ~1.6–3.2 μm). The size of the selected area over which the diffusion coefficient is averaged depends on the value of the diffusion coefficient and of the speed of scanning.

TABLE 3 Repetitions of the same simulation ($N = 10$) to estimate standard deviations

Method (data acquired at 16 μs per point)	D in $\mu m^2/s$	G(0)
Single point FCS (Eq. 7)	2.6 ± 0.9	1.7 ± 0.4
Circular scan (Eq. 6)	2.5 ± 0.1	1.6 ± 0.1
Circular scan (128 points per orbit) Eq. 8	2.5 ± 0.3	1.5 ± 0.1
Raster scan (128 × 128 pixels) Eq. 10	2.5 ± 0.3	1.5 ± 0.1

100 particles diffusing in a plane of 128 × 128 pixels of 0.05 μm each detected by different methods and recovered by the different equations in the text. The length of the data stream is the same for each simulation; 320,000 points were simulated.

Line (or circular) scan versus raster images

The main advantage of the circular scan pattern is that it gives the fastest possible sustained scan motion that can be obtained with mechanical scanners. It gives a continuous stream of data in time. Extracting diffusion coefficients from the continuous data time series and looking at single locations for successive scan orbits has been described (9,16).

TABLE 4 Order of magnitude of diffusion coefficients that can be determined by spatial and time correlation using laser scanning systems

Recovered by spatial correlation	D $\mu m^2/s$	Time to adjacent point	Method
	100	0.1 ms	Pixel, line or raster scanning
	10	1 ms	Pixel, line or raster scanning
	1	10 ms	Line, raster scanning
	0.1	100 ms	Line, raster scanning
	0.01	1000 ms	Impractical
	0.001	10,000 ms	Impractical
Recovered by temporal correlation	D $\mu m^2/s$	Time at same point	Method
	100	<0.01 ms	Point FCS
	10	<0.1 ms	Point and line scanning
	1	<1 ms	Point and line scanning
	0.1	<10 ms	Point and line scanning
	0.01	<100 ms	Line and fast raster scanning
	0.001	<1000 ms	Raster scan with temporal ICS

What has not been described previously is the information that can be extracted by performing spatial correlation of points along the scan orbit. We presented two different aspects of the spatiotemporal correlation approach, one for line scanning and the other for raster-scan images. Although the two methods are mathematically treated in the same framework and the equations describing spatial autocorrelation functions are similar for line scan and for raster scan, there is an important practical difference between the two. Line scan allows very high temporal and spatial resolution. At the pixel level resolution, the temporal resolution of the line-scan method depends on the scan-line repetition time. For raster images, high spatial resolution (pixel level resolution) for dynamic processes can only be obtained for millisecond dynamics. However, information on the fast dynamics can be obtained from the pixels along a line, but the spatial resolution is reduced. Table 5 describes the spatial resolution that can be obtained for different methods of data acquisition. In principle, both methods (line scan and raster image) can be implemented in any commercial LSM. In regard to the total time of data acquisition needed for this technique, the data set used for Figs. 5 and 6 has 23 frames taken at 512 × 512 frame size with a pixel time of 8 μs, giving a total acquisition time of <1 min. The data set used to analyze the dynamics in Fig. 7 along one line has 10,000 lines for a total acquisition time of 54 s.

TABLE 5 Resolution of the various scan methods

Method	Temporal resolution	Spatial resolution
Line or circular scan	Millisecond	Pixel resolution (submicron)
Raster scan	Microsecond	Low resolution (typically 16 or 32 pixels), depends on the particle diffusion coefficient and the scan speed. Generally we operate at 0.092 μm/pixel.
Frame scan	Second	Pixel resolution (submicron)

Subtracting immobile features

Perhaps the most striking difference between single-point FCS and the RICS method is the inherent capability of RICS to filter out bright immobile or slowly moving features. In addition, the RICS method simultaneously provides dynamic information as well as an image of the cell. This allows one to retrospectively choose regions of the cell that are interesting and focus analysis in these areas. In contrast, with single-point FCS measurements it is very difficult to know exactly which volume in the cell was measured, and this is especially true if the cell is moving during the measurement. It is important that the regions chosen for analysis be relatively homogeneous. Since the diffusion coefficient obtained from the fit refers to an average value of the region analyzed, this region should not cross membranes or other clear divisions in the cell.

The focus of this article is to illustrate how different methods can be used to obtain diffusion and dynamics. However, the fluorophore concentration can also be extracted from solution samples if we know the focal volume from the inverse of the autocorrelation function amplitude, $G(0)$, obtained using the different methods. Table 2 shows that the same value of $G(0)$ is obtained applying the different equations for data analysis. In the presence of bright immobile structures, when the subtraction algorithm is applied the relationship between $G(0)$ and number of particles is no longer valid.

Other dynamic processes

There are large intensity fluctuations at the immobile spots in an image. These fluctuations can be due to shot noise or to other dynamic processes such as binding equilibria, dynamic quenching, changes in conformations, rotational dynamics, dynamic fluorescence resonance energy transfer, and many other process that alter the fluorescence. By measuring the temporal and spatial correlation at the bright spots we can distinguish between shot noise and fluctuations due to dynamic processes. For example, it is probable that the dynamics we observe for paxillin-EGFP localized in adhesions are due to binding equilibria rather than diffusion of large aggregates. We are developing models to fit the data to distinguish among the different physical processes occurring at the adhesions. For example, binding equilibria have an exponential correlation (in time) rather than the characteristic

form for diffusion (Eq. 7). Preliminary fits of the correlation functions obtained from the experiment in Fig. 7 show that, indeed, at the adhesions this model was a better fit to the experimental data. The best approach to distinguish between diffusion and localized processes is to change the waist of the excitation beam. Distinguishing diffusion from binding is beyond the scope of this article and will be discussed in detail elsewhere.

CONCLUSIONS

RICS is a novel image-analysis technique that uncovers the hidden dynamic information within each image collected on an LSM. The beauty of the technique is that it allows one to measure the dynamics of soluble cytosolic proteins, membrane-associated proteins, slow moving transmembrane proteins, multiprotein complex dynamics, and protein binding equilibria from a single image time series. Importantly, these measurements can even be done in the presence of large immobile features commonly found in the cell. The accessible timescales span all the way from microseconds to seconds. We essentially present software for data analysis that, with the proper mathematical analysis, can expose the intrinsic time structure that is contained in every LSM image. The method gives accurate measurements of diffusion coefficients, comparable to expensive single-point FCS instruments. This opens up these types of measurements to any confocal microscope user. The impact within the life sciences community to the study of protein dynamics over orders of magnitude in time within living cells should be huge.

Work supported in part by Cell Migration Consortium grant No. U54 GM064346 (to M.D., A.H., C.B., and E.G.), National Institutes of Health grant No. P41-RRO3155 (to E.G. and P.S.), and the Natural Sciences and Engineering Research Council of Canada and the Canadian Institutes of Health Research (to P.W.W.).

REFERENCES

1. Ridley, A. J., M. A. Schwartz, K. Burridge, R. A. Firtel, M. H. Ginsberg, G. Borisy, J. T. Parsons, and A. R. Horwitz. 2003. Cell migration: integrating signals from front to back. *Science*. 302: 1704–1709.
2. Wiseman, P. W., C. M. Brown, D. J. Webb, B. Herbert, N. L. Johnson, J. A. Squier, M. H. Ellisman, and A. R. Horwitz. 2004. Spatial mapping of integrin interaction and dynamics during cell migration by image correlation spectroscopy. *J. Cell Sci.* 117: 5521–5534.
3. Xie, S. 2001. Single-molecule approach to enzymology. *Single Mol.* 4:229–236.
4. Moerner, W. E., and M. Orrit. 1999. Illuminating single molecules in condensed matter. *Science*. 283:1670–1676.
5. Weiss, S. 1999. Fluorescence spectroscopy of single biomolecules. *Science*. 283:1676–1683.
6. Herbert, B., S. Costantino, and P. W. Wiseman. 2005. Spatiotemporal image correlation spectroscopy (STICS) theory, verification and application to protein velocity mapping in living CHO cells. *Biophys. J.* 88:3601–3614.
7. Magde, D., E. Elson, and W. W. Webb. 1972. Thermodynamic fluctuations in a reacting system—measurement by fluorescence correlation spectroscopy. *Phys. Rev. Lett.* 29:705–708.
8. Elson, E. L., and D. Magde. 1974. Fluorescence correlation spectroscopy. I. Conceptual basis and theory. *Biopolymers*. 13:1–27.
9. Berland, K. M., P. T. So, and E. Gratton. 1995. Two-photon fluorescence correlation spectroscopy: method and application to the intracellular environment. *Biophys. J.* 68:694–701.
10. Petersen, N. O., P. L. Hödelius, P. W. Wiseman, O. Seger, and K. E. Magnusson. 1993. Quantitation of membrane receptor distributions by image correlation spectroscopy: concept and application. *Biophys. J.* 65:1135–1146.
11. Wiseman, P. W., J. A. Squier, M. H. Ellisman, and K. R. Wilson. 2000. Two-photon video rate image correlation spectroscopy (ICS) and image cross-correlation spectroscopy (ICCS). *J. Microsc.* 200: 14–25.
12. Petersen, N. O., C. M. Brown, M. Srivastava, J. Rocheleau, and P. W. Wiseman. 1998. Analysis of membrane protein cluster densities and sizes by in situ image correlation spectroscopy. *Faraday Disc.* 111: 289–305.
13. Digman, M. A., P. Sengupta, P. W. Wiseman, C. M. Brown, A. R. Horwitz, and E. Gratton. 2005. Fluctuation correlation spectroscopy with a laser-scanning microscope: exploiting the hidden time structure. *Biophys. J.* 88:L33–L36.
14. Berland, K. M., P. T. So, Y. Chen, W. W. Mantulin, and E. Gratton. 1996. Scanning two-photon fluctuation correlation spectroscopy: particle counting measurements for detection of molecular aggregation. *Biophys. J.* 71:410–420.
15. Magde, D., W. W. Webb, and E. L. Elson. 1978. Fluorescence correlation spectroscopy. III. Uniform translation and laminar flow. *Biopolymers*. 17:361–376.
16. Ruan, Q., Y. Chen, E. Gratton, M. Glaser, and W. W. Mantulin. 2002. Cellular characterization of adenylate kinase and its isoform: two-photon excitation fluorescence imaging and fluorescence correlation spectroscopy. *Biophys. J.* 83:3177–3187.